Proceedings of the 9th International Conference on Fluid Flow, Heat and Mass Transfer (FFHMT'22)
Niagara Falls, Canada – June 08-10, 2022
Paper No. 189
DOI: 10.11159/ffhmt22.189

Numerical Investigation on the Geyser Boiling in High Temperature Wick Sodium Heat Pipe based on CFD method

Dahai Wang, Fangjun Hong
School of Mechanical Engineering, Shanghai Jiao Tong University
Shanghai, 200240, China;
First. dahai_wang@sjtu.edu.cn; Second. mehongfj@sjtu.edu.cn

Abstract **-** In order to analyze the geyser boiling phenomenon in high temperature wick sodium heat pipe, it is used as a numerical simulation method for safety analysis of high temperature heat pipe system. The geyser boiling phenomenon of high temperature sodium heat pipe was analyzed by using Volume of fluid (VOF) model and capillary force model. The process of bubble nucleation, growth, polymerization, and separation from the wall in the liquid pool of heat pipe evaporation section, as well as the backflow phenomenon of capillary suction in the wick were obtained by numerical calculation, which verified the accuracy and stability of capillary force model in the wick. In addition, the causes of geyser boiling of heat pipes were analyzed by extracting oscillating temperature distribution of heat pipe wall. The results show that the speed of bubble separation and the timely reflow of liquid sodium (condensate) in the wick play a key role in the periodic oscillation of tube wall temperature. Therefore, the numerical simulation method established in this study can provide reference for transient calculation of geyser boiling of sodium heat pipes.

Keywords**:** Sodium heat pipe; Geyser boiling; Volume of fluid; Capillary

1. Introduction

High-temperature heat pipe is often used for thermal protection of supersonic aircraft, space nuclear reactor cooling and other fields due to its advantages of high thermal conductivity, non-dynamic characteristics, high thermal efficiency and low weight [1]. Liquid metals, such as lithium, sodium, or potassium, are usually selected as working fluids for high-temperature heat pipe. Nuclear boiling in the liquid pool area of evaporation section of high-temperature heat pipe leads to periodic nucleation, growth, polymerization, separation from the wall and overflow of bubbles, resulting in periodic oscillations of internal pressure, liquid surface position and wall temperature [2]. It is important for the design and safe operation of high-temperature heat pipe to explore the operation characteristics of heat pipe under geyser boiling condition.

At present, a large number of experimental studies [3, 4] have found that the temperature of the tube wall will periodically oscillate at a certain power. However, based on the characteristics of heat pipe, it is difficult to observe the internal two-phase flow field information and dynamic characteristics through experimental methods. Therefore, it is necessary to analyse the internal flow field characteristics of heat pipe under transient operating condition by means of numerical model. Cao and Faghri et al. [5, 6] proposed a two-zone model for the start-up process of high-temperature heat pipes. Compressible Navier-Stokes equations are used for continuous steam and mass self-diffusion equations for rarefied steam. Alizadehakhl et al. [7] successfully simulated a two-phase closed thermal siphon using the volume of fluid (VOF) model in Fluent. It is proved that the calculation model can be applied to the phase transformation of a single heat pipe during evaporation and condensation. Ranjan et al. [8] established a transient three-dimensional heat pipe heat transfer model. The relationship between the evaporation rate and the liquid film form in the pores on the surface of the wick structure was analysed. However, most of the current researches using two-phase CFD simulation are aimed at heat pipes with low temperature working medium. Transient calculation and simulation of high-temperature heat pipe mainly focus on the heat pipe start-up and one-dimensional heat transfer characteristics, but few researchers pay attention to the geyser boiling phenomenon of high-temperature heat pipe.

Therefore, based on the simulation model of VOF multiphase flow, this paper studies the geyser boiling of high-temperature wick sodium heat pipe. Combined with vapor dynamics model and porous model, boiling evaporation model

and capillary force model in high temperature sodium heat pipe are proposed. In addition, the heat transfer and flow characteristics of three-dimensional heat pipes under different heat transfer powers and dip angles were studied.

2. Numerical Model

Figure 1 shows the working principal diagram of a typical high-temperature wick sodium heat pipe. High-temperature heat pipes are divided into nuclear boiling region and thin liquid film evaporation condensation region. The capillary force of the heat pipe provides reflux.

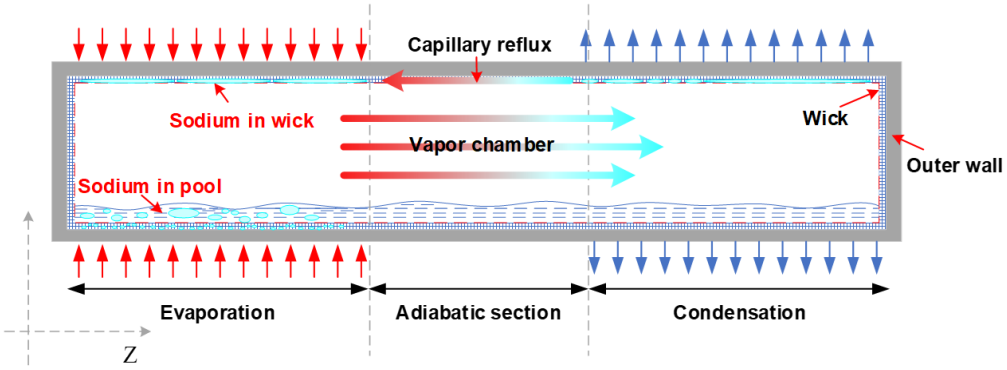

Fig. 1 Schematic diagram of working principle of high-temperature wick sodium heat pipe

2.1. Mesh geometry

The total length of the heat pipe is 100 mm, the inner diameter is 16 mm, the wall thickness is 2 mm, the thickness of the wick is 0.3 mm, including evaporation section of 20 mm, adiabatic section of 60 mm, condensation section of 20 mm. The specific geometric model is shown in Figure 2. In terms of grid, variable spacing boundary layer grid is adopted for the grid division of the wick and the internal fluid area. The initial grid spacing is set as 0.03mm, and the growth ratio is 1.1, and it is divided into 12 layers. Finally, 562764 grids were selected.

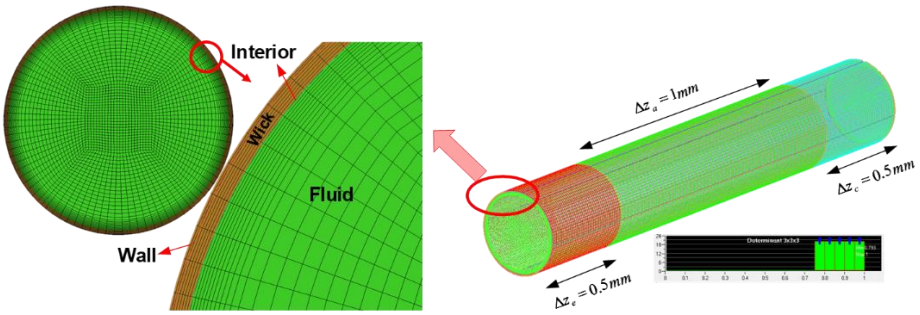

Fig. 2 The employed mesh geometry in the modeling

2.2. Governing equations

In the vapor-liquid two-phase VOF model, α_v and α_l are used to represent the volume percentage of the vapor phase and liquid phase in the calculation cell, respectively. All the calculation cells are filled with one or two components. The continuity, momentum and energy governing equations used to simulate heat transfer and flow field are as follows:

Continuity equation:

$$\begin{cases} \nabla \cdot (\alpha_v \rho_v \vec{u}) = -\varepsilon \dfrac{\partial}{\partial t}(\alpha_v \rho_v) + S_{m,v} \\ \nabla \cdot (\alpha_l \rho_l \vec{u}) = -\varepsilon \dfrac{\partial}{\partial t}(\alpha_l \rho_l) + S_{m,l} \end{cases} \tag{1}$$

In the formula, ε represents the porosity of the wick, and when ε=1 represents the mass conservation equation of the working medium in the steam chamber. Where $S_{m,v}$ and $S_{m,l}$ are the mass source terms of the vapor phase and liquid phase respectively, which can be quantitatively given by the following equation according to the relationship between local temperature and saturation temperature:

$$\textit{Evaporation}\begin{cases} S_{m,v} = r_e \alpha_l \rho_l \dfrac{T_{mix} - T_{sat} - \Delta T}{T_{sat}} \\ S_{m,l} = -r_e \alpha_l \rho_l \dfrac{T_{mix} - T_{sat} - \Delta T}{T_{sat}} \end{cases} \quad ,T_{mix} > T_{sat} \tag{2}$$

$$\textit{Condensation}\begin{cases} S_{m,v} = -r_c \alpha_v \rho_v \dfrac{T_{sat} - T_{mix} - \Delta T}{T_{sat}} \\ S_{m,l} = r_c \alpha_v \rho_v \dfrac{T_{sat} - T_{mix} - \Delta T}{T_{sat}} \end{cases} \quad ,T_{sat} > T_{mix} \tag{3}$$

Where r_e and r_c represent evaporation and condensation coefficients respectively, representing the speed of evaporation and condensation. The grid unit is used to monitor the vapor-liquid interface to see if it meets the saturation pressure range, and the two coefficients are gradually modified to make it closer to the real situation. After debugging, the evaporation coefficient is 10, and the condensation coefficient is 50000.

Momentum equation:

$$\frac{\partial}{\partial t}(\rho\vec{v}) + \nabla\cdot(\rho\vec{v}\vec{v}) = -\varepsilon\nabla p + \nabla\cdot\left[\mu(\nabla\vec{v} + \nabla\vec{v}^T) - \frac{2}{3}\mu\nabla\cdot\vec{v}I\right] - \frac{\mu\varepsilon}{K}u - \frac{C_E\varepsilon}{K^{\frac{1}{2}}}\rho\left|\vec{V}\right|u + \rho\vec{g} + F_{csf} + F_{cap} \tag{4}$$

In the above equation, the fifth term on the right represents the gravitational source term. The fourth term on the right represents the pressure loss due to the inertial resistance of the fluid, and C_E represents the Ergun coefficient. The third term on the right of the equation represents the viscous resistance of fluid flow in the wick, that is, the pressure loss caused by Darcy's infiltration. When ε=1 and K=∞, the momentum conservation equation of working medium flow in the steam chamber is expressed. The calculation formula for the screen porosity and permeability [9] in the wick is as follows:

$$\begin{cases} \varepsilon = 1 - \dfrac{2\pi\left(d_{wick,1}^{2}N_1 + d_{wick,2}^{2}N_2\right)}{101.6 \times h_{wick}} \\ K = \dfrac{d_{wick}^2\varepsilon^3}{122(1-\varepsilon)^2} \end{cases} \tag{5}$$

F_{csf} is the continuous surface force proposed by Brackbill et al. [10], which is used to consider the surface tension near the vapor-liquid interface on the solid wall, and can be obtained by:

$$F_{csf} = 2\sigma_{lv}\frac{\alpha_l\rho_l C_v\nabla\alpha_v + \alpha_v\rho_v C_l\nabla\alpha_l}{\rho_l + \rho_v} \tag{6}$$

In order to simulate the phenomenon of capillary reflux, the capillary force model F_{cap} needs to be added to the momentum equation. Figure. 3 shows the schematic diagram of capillary drive in the wick.

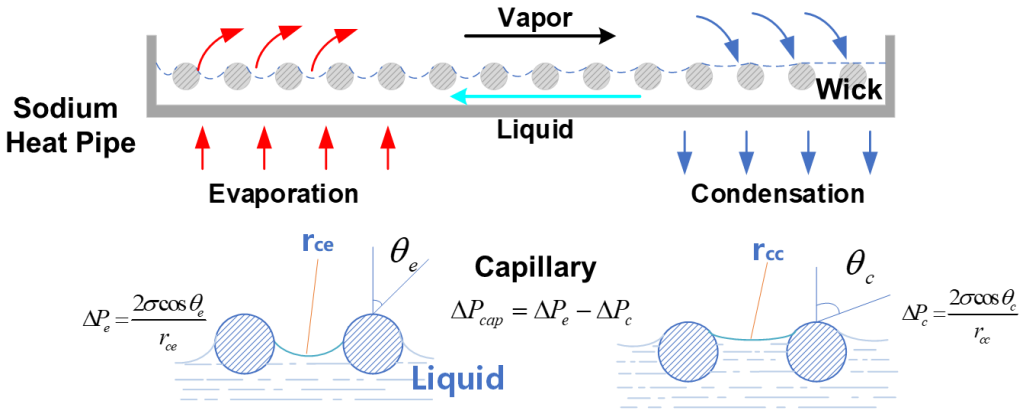

Fig. 3 Capillary drive diagram of wick

In the process of calculation, the maximum capillary pressure difference that can be provided by the screen of the wick and the average value of the phase volume difference of VOF in the calculation unit are extracted (Equation 8), and the gradient of the phase volume fraction is extracted (Figure. 4 (a)), so as to represent the changing direction of the curvature of the vapor-liquid interface. Capillary pressure drags the vapor-liquid interface toward the vaporeous side.

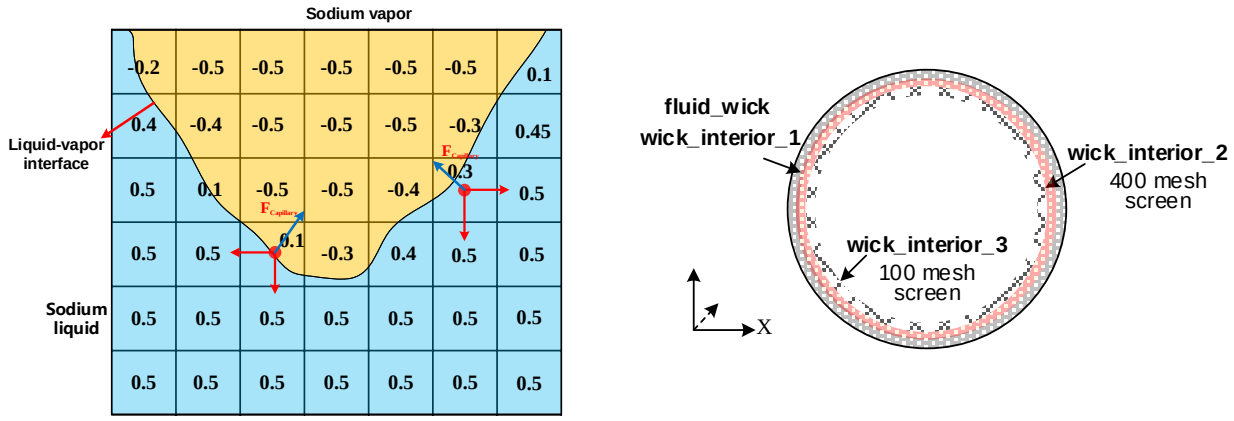

(a) VOF phase volume fraction gradient (b) Diagram of capillary wick partition

Fig. 4 Capillary force model in wick

In addition, the area of the wick is calculated by partition, as shown in Figure. 4 (b). For the two-layer grid (WICK_interior_1) near the solid wall area, the F_{csf} model embedded in FLUENT is used (surface tension of sodium: 0.129; Contact Angle: 5°). Add the F_{cap} model for the other areas (wick_interior_2/3).

Energy equation:

$$\frac{\partial}{\partial t}(\varepsilon\rho E) + \nabla\cdot(\vec{v}(\rho E + p)) = \nabla\cdot(k_{eff}\nabla T) + S_e \tag{7}$$

$$\begin{cases} \vec{a} = \dfrac{\left(a_l - a_v\right)}{2} \\ \nabla\vec{a}\begin{cases} \cos\theta \cdot \partial\vec{a} / \partial x \\ \cos\theta \cdot \partial\vec{a} / \partial y \\ \cos\theta \cdot \partial\vec{a} / \partial z \end{cases} \\ \Delta P_{cap,i} = -\dfrac{4\sigma\cos\theta}{d_{silk}} \dfrac{\partial\vec{a}}{\partial x_i} \end{cases} \tag{8}$$

2.3. Capillary force model validation

In order to verify the correctness and stability of capillary force model in three-dimensional computational domain, the flow state of liquid sodium in the wick of heat pipe without capillary force model was calculated first. It can be seen from Figure. 5 (a) that when T=0.08s, there are obvious droplet drops at the position of the upper wick. It indicates that without capillary force, the liquid in the upper wick will gradually return to the liquid pool area. By adding the capillary force model to the momentum source term, Figure. 5 (b) shows that within the same calculation time, after adding the capillary force, there is no liquid sodium disengagement in the wick region, and the interface position will be automatically adjusted at the vapor-liquid interface due to the action of the capillary force.

(a) No capillary force is added (b) Add (X/Y/Z direction) capillary force

Fig. 5 3D capillary force model validation

In addition, the initial start-up state of liquid sodium in the heat pipe is simulated. Due to capillary suction, the working medium sodium in the liquid pool flows along the wick. Finally, the wick is filled with saturated liquid sodium (Figure. 6).

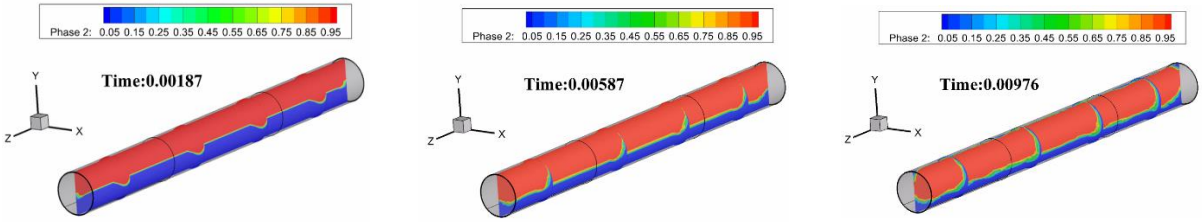

Fig. 6 Heat pipe capillary start process

3. Results And Discussion

The flow pattern distribution and temperature oscillation of the pipe wall surface of the horizontal and 15 Angle heat pipe are analysed under the power of 800W (heat flux is kept at 3000W /m^2) and transient operation. The boundary conditions of air cooling in the condensation section are as follows: the natural convective coefficient is 6.03 W/(m^2·K), and the surface radiant emissivity of the condensation section is 0.65.

3.1. Temperature oscillation phenomenon in horizontal heat pipes

Figure. 7 (a) shows the initialization state of three-dimensional heat pipe. Boiling model is added to the liquid pool area of evaporation section, and evaporation model is added to the vapor-liquid interface of liquid wick. A condensation model was added at the vapor-liquid interface between the liquid pool area of the condensation section and the wick. In addition, the capillary force model was loaded in the wick region of the liquid tank.

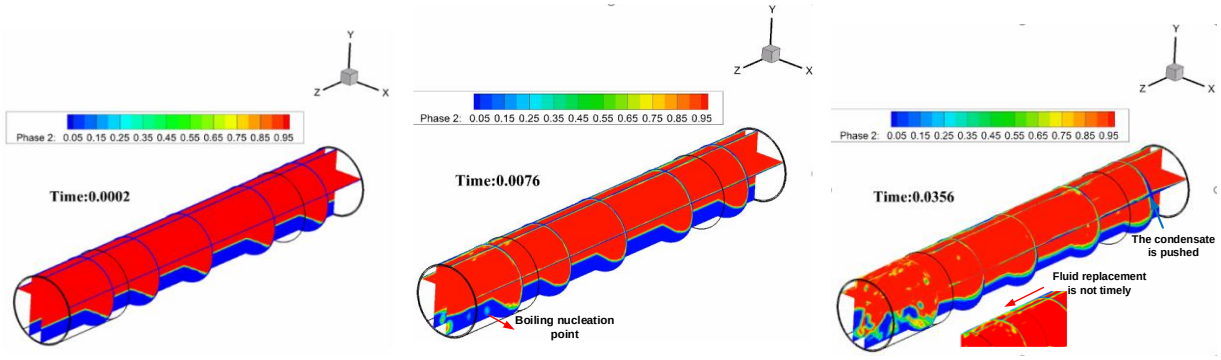

(a) The heat pipe is initialized (b) Nuclear boiling phenomenon (c) Capillary reflux

Fig. 7 Phase distribution in 3D heat pipe

Figure. 7 (b) shows the process of bubble nucleation, growth, polymerization and separation from the wall in the liquid pool of evaporation section. In the evaporation section, evaporation occurs at the vapor-liquid interface between the liquid pool and the wick. When the wall superheat exceeds the set temperature 15℃, the gasification core randomly generated on the wall begins to produce bubbles, and the bubbles generated by the gasification core do not interfere with each other. With the increase of superheat, the core of gasification will increase, and the bubbles will influence each other and coalesce into vapor blocks and columns. During the boiling process, the temperature of the wall surface will rise sharply as the bubble detach from the wall surface. In the upper wick area, the evaporation of vapor-liquid interface will cause the vapor-liquid interface to retreat into the wick, and at this time, the capillary pressure drags the vapor-liquid interface to the gaseous side. Found in the figure 8 (c) as the computing time further, in the process of pool boiling, interface, provide capillary force cannot lead to absorb liquid core in a timely manner the rehydration process, make the liquid in the period of local drought, liquid sodium to appear if the rehydration less will cause on the surface of the tube wall temperature rising sharply.

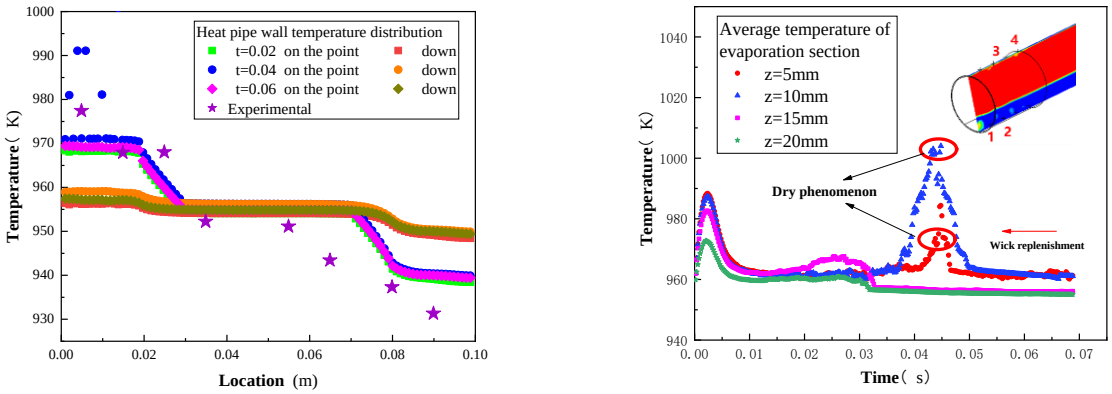

(a) (b)

Fig. 8 The change of temperature field of tube wall

Figure 8 (a) shows that the average temperature difference between the evaporation section and the condensation section is about 18-20℃, and the temperature of the adiabatic section corresponds to the experimental data and is close to the saturation temperature in the heat pipe. According to the data of the measurement points on the evaporation section,

the temperature of the tube wall in some positions is too high, and there is a phenomenon of dry burning and lack of liquid, indicating that the liquid sodium fails to replenish the wetting wall in time, or the capillary force has not had time to replenish the wetting wall, leading to the wall temperature rise here.

It can be seen from Figure. 8 (b) that the fluctuation of average temperature above and below 3/4 of the measuring point is small, and the wall temperature increases significantly in the boiling process, and fluctuates in small amplitude in the subsequent calculation time. For the 1/2 measuring point, the wall temperature began to rise sharply from 0.035, indicating that the phenomenon of liquid shortage began to appear here. At this time, the superheat of the wall would have a temperature difference of 40-50℃, and the tube wall temperature began to decline with the replenishments.

3.2. Inclination influence on the temperature oscillations

Figure.9 shows the phase distribution in the heat pipe with an inclination Angle of 15°. After the calculation and stabilization, the liquid is concentrated in the position of the evaporation section, and the wick is filled with liquid sodium under the action of capillary force. However, in the upper part of the evaporation section, the dry burning phenomenon occurs in the wick due to the violent fluctuation of boiling interface. This has the same phenomenon as horizontal placement, but under the combined action of gravity and capillary force, liquid sodium in the liquid pool will timely infiltrate the upper wick. By extracting the average temperature distribution of the liquid pool area on the heat pipe wall at different times, analysing the calculation measurement points of evaporation section and analysing its dynamic change, extracting the average temperature of the upper and lower top section of the tube wall at 5mm and 10mm respectively, and the characteristics of the tube wall temperature change with the calculation time.

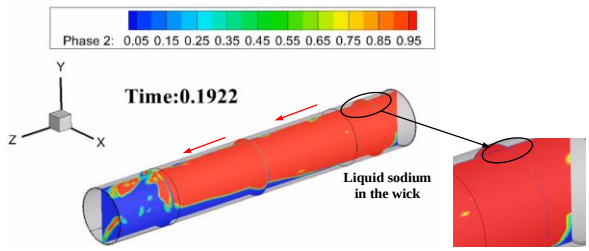

Fig. 9 3D heat pipe incline 15° tube phase distribution

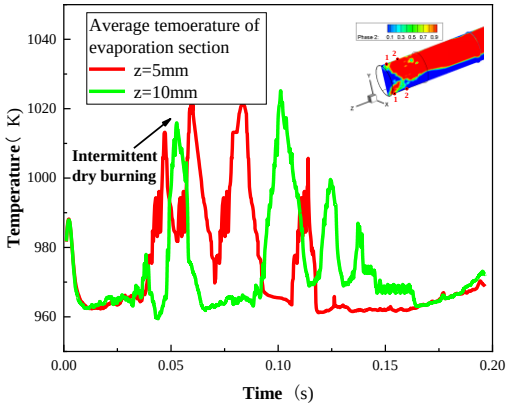

Fig. 10 The average temperature of pipe wall changes at different time

Figure.10 shows the change of tube wall temperature with time at measuring points (5 and 10mm) in evaporation section. It can be found that the temperature of the tube wall fluctuates geyserly, and the temperature fluctuation range is 40-50℃. The sharp rise of the temperature of the tube wall indicates that dry burning occurs here. With the supplement of liquid sodium in the wick, the temperature of the tube wall begins to drop. Geyser temperature oscillations occur with the process of evaporation, boiling and rehydration. The time of oscillation depends on the speed of rehydration of the wick, and is proportional to the size of the capillary force applied. After 0.15s, it is found that the amplitude of wall temperature oscillation decreases, indicating that the wick is full of liquid sodium and there is no liquid shortage phenomenon temporarily.

In the results of three-dimensional simulation calculation, it is found that the bubble separation is affected by the screen pore size, after the bubble nucleation, it is difficult to detach, the bubble is fixed on the surface, easy to form a massive gas film covering the surface of the tube wall, resulting in local dry burning, thereby triggering geyser boiling instability. In the actual experiment, it is difficult for the bubble to detach from the wick, which leads to a sharp rise in temperature. Once the bubble detach, the surrounding liquid is moistened in time, which leads to a drop in the temperature of the tube wall and the next cycle.

4. Conclusion

In this study, VOF two-phase CFD analysis method was used to calculate geyser boiling transient of high temperature sodium heat pipe, and the following conclusions were obtained through simulation:

(1) The development of capillary force model in the wick. The process of bubble nucleation, growth, polymerization and separation from the wall can be simulated by using VOF method and boiling evaporation model, as well as the backflow phenomenon of capillary suction in the wick.

(2) Comparing the CFD simulation results in this paper with the sodium experiment results at 800 W heating power, the error between the experimental results in the evaporation section and the adiabatic section and the simulation results is less than 10 ℃, which verifies the rationality of the CFD calculation model in this paper.

(3) The fluctuation of temperature field on the wall surface of high temperature sodium heat pipe with time was analyzed. During the boiling process, the bubbles failed to break away from the tube wall in time, and the wall surface appeared local dry burning, accompanied by the rapid rise of wall temperature. With the replenishment of liquid sodium (condensate) in the wick, the temperature of the tube wall begins to drop. The periodic oscillation of wall temperature was formed by the cyclic process of dry burning - temperature rise - filling and wetting of wick - dry burning.

References

[1] A. Faghri, "Review and advances in heat pipe science and technology," *Journal of Heat Transfer,* vol. 134, 2012-01-01 2012.

[2] Y. Ma, H. Yu, S. Huang, Y. Zhang, Y. Liu, C. Wang, R. Zhong, X. Chai, C. Zhu, and X. Wang, "Effect of inclination angle on the startup of a frozen sodium heat pipe," *Applied Thermal Engineering,* vol. 201, 2022-01-01 2022.

[3] W. Teng, X. Wang and Y. Zhu, "Experimental investigations on start-up and thermal performance of sodium heat pipe under swing conditions," *International Journal of Heat and Mass Transfer,* vol. 152, 2020-01-01 2020.

[4] H. X. Chen, Y. X. Guo, D. Z. Yuan, and Y. Ji, "Experimental study on frozen startup and heat transfer characteristics of a cesium heat pipe under horizontal state," *International Journal of Heat and Mass Transfer,* vol. 183, 2022-01-01 2022.

[5] A. Faghri, "Heat pipe science and technology," *Fuel & Energy Abstracts,* vol. 36, p. 285-285, 1995.

[6] Y. Cao and A. Faghri, "Transient multidimensional analysis of nonconventional heat pipes with uniform and nonuniform heat distributions," *Journal of Heat Transfer,* vol. 113, pp. 995-1002, 1991.

[7] A. Alizadehdakhel, M. Rahimi and A. A. Alsairafi, "CFD modeling of flow and heat transfer in a thermosyphon," *International Communications in Heat and Mass Transfer,* vol. 37, pp. 312-318, 2010.

[8] R. Ranjan, J. Y. Murthy and S. V. Garimella, "A microscale model for thin-film evaporation in capillary wick structures," *International Journal of Heat and Mass Transfer,* vol. 54, pp. 169-179, 2011-01-01 2011.

[9] H. Sun, S. Tang, C. Wang, J. Zhang, D. Zhang, W. Tian, S. Qiu, and G. Su, "Numerical simulation of a small high-temperature heat pipe cooled reactor with CFD methodology," *Nuclear Engineering and Design,* 2020-01-01 2020.

[10] J. U. Brackbill, D. B. Kothe and C. Zemach, "A continuum method for modeling surface tension," *Journal of Computational Physics,* vol. 100, pp. 335-354, 1992-01-01 1992.